Resonant MEMS Tunable VCSEL

Thor Ansbæk, Il-Sug Chung, Elizaveta S. Semenova, Ole Hansen, and Kresten Yvind

***Abstract*—We demonstrate how resonant excitation of a microelectromechanical system can be used to increase the tuning range of a vertical-cavity surface-emitting laser twofold by enabling both blue- and red-shifting of the wavelength. In this way, a short-cavity design enabling wide tuning range can be realized. A high-index-contrast subwavelength grating vertical-cavity surface-emitting laser with a monolithically integrated antireflection coating is presented. By incorporating an antireflection coating into the air cavity, higher tuning efficiency can be achieved at low threshold current. The first result shows 24-nm continuous resonant tuning range around an emission wavelength of 1060 nm with 0.9 mW output power.**

***Index Terms*—III-V semiconductor materials, microelectromechanical systems, semiconductor lasers, vertical cavity surface emitting lasers.**

I. Introduction

SEMICONDUCTOR lasers emitting at a wavelength of 1060 nm have potential applications within short-reach optical interconnects and medical diagnostics [1], [2]. For optical interconnects, vertical-cavity surface-emitting lasers (VCSELs) have already been established as the attractive choice where low-power consumption and high volume is desired. For sensing applications, VCSELs are also a popular choice offering low power consumption and good spectral properties [3], [4].

Optical coherence tomography (OCT) is a well-established medical diagnostic technique for cross-sectional imaging of the retina, which is part of the eye. In the field of OCT, it has been recognized that imaging at 1060 nm, instead of the current standard of 840 nm, enables visualization of the choroidal vascular structure [5], [6]. This has important clinical implications in imaging the retina on patients with cataract. Air-cavity tunable VCSELs enable the broadband tunability required for high-resolution OCT imaging [2].

A VCSEL with an air-cavity can provide much greater wavelength tunability than solid-cavity VCSELs [7], [8]. Temperature-induced wavelength tuning is a well-known effect in semiconductor lasers, but the tuning range is limited. The widest tuning range reported so far is 10 nm at an emission wavelength of 950 nm [9]. In contrast 102 nm tuning range at 1550 nm, 142 nm at 1310 nm, and 90 nm at 1060 nm has been reported for air-cavity tunable VCSELs with electrical or optical pumping [10]–[12]. These designs are limited in tuning range by the free spectral range (FSR). The FSR can be increased by decreasing the optical cavity length, but this will also reduce the wavelength tuning range.

We show that when the tuning is provided by a mirror realized in a resonant microelectromechanical system (MEMS) the tuning range can be increased by exciting the MEMS structure at resonance. The increased tuning range results from the bipolar motion of the mirror around the rest position; as a result red- as well as blue-shifting of the laser wavelength is accomplished.

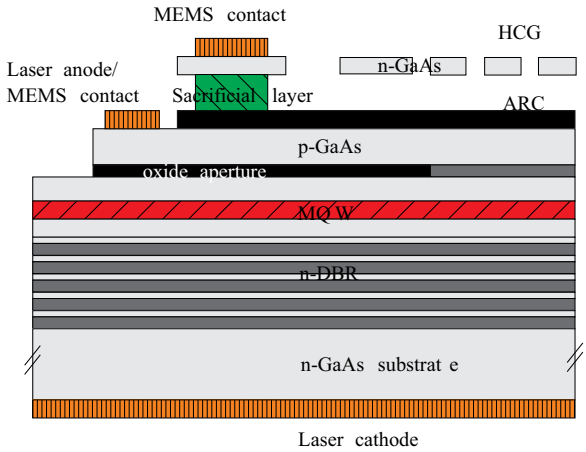

Fig. 1. Schematic drawing of the epitaxial structure of the tunable MEMS VCSEL.

II. Device Structure

The structure of the tunable MEMS VCSEL, shown in Fig. 1, includes an electrostatically actuated mirror for laser wavelength tuning; the mirror is integrated with the laser cavity and gain medium in a monolithic unit. The structure is a half-VCSEL with an intracavity contact. An air gap between the half-VCSEL and the top mirror makes it possible to change the physical cavity length. On top of the intracavity contact a low-refractive index oxide is placed, such that the reflection at the air-semiconductor interface is reduced and an extended cavity design achieved. The optical cavity length, nL, is five times the distributed Bragg reflector (DBR) wavelength λ_B. We have chosen the extended cavity design since this configuration has the best tradeoff between threshold material gain and tuning efficiency [8]. In order to achieve a polarization stable output, we have chosen to replace the top distributed Bragg reflector (DBR) with a high index contrast grating (HCG) mirror. In contrast to the earlier design by Huang *et al*. [13] we omit the p-doped DBR, since this

Manuscript received October 31, 2012; revised January 8, 2013; March 20, 2013; accepted March 25, 2013.

T. Ansbæk, I.-S. Chung, E. S. Semenova, and K. Yvind are with the DTU Fotonik, Department of Photonics Engineering, Technical University of Denmark, Ørsteds Plads, 2800 Kongens Lyngby, Denmark (e-mail: tans@fotonik.dtu.dk; ilch@fotonik.dtu.dk; esem@fotonik.dtu.dk; kryv@fotonik.dtu.dk).

O. Hansen is with the DTU Nanotech, Department of Micro- and Nanotechnology, and CINF, Center for Individual Nanoparticle Functionality, Technical University of Denmark, Ørsteds Plads, 2800 Kongens Lyngby, Denmark (e-mail: ole.hansen@nanotech.dtu.dk).

Color versions of one or more of the figures in this paper are available online at http://ieeexplore.ieee.org.

Digital Object Identifier 10.1109/JSTQE.2013.2257164

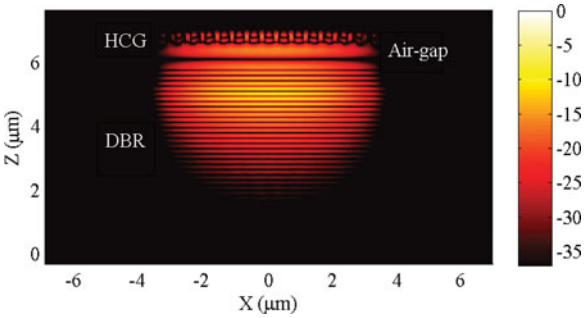

Fig. 2. Calculated optical mode profile of the fundamental mode (intensity plotted in dB-scale).

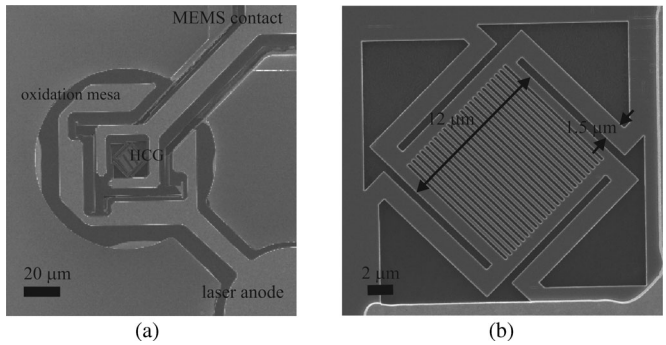

Fig. 3. Scanning electron micrographs of the fabricated VCSEL. The full VCSEL structure is shown in (a), while (b) shows a close-up of the MEMS structure and the HCG mirror.

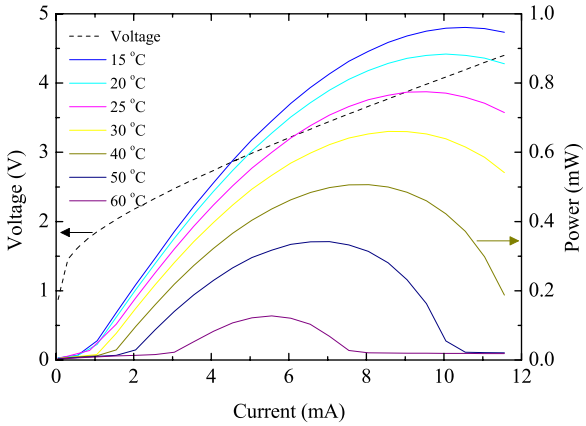

Fig. 4. Plot of the voltage (left axis, dashed line) and optical intensity (right axis, solid line) as a function of VCSEL current.

will introduce an undesired reflection that will limit the continuous tuning range [14]. The bottom n-doped DBR mirror has 35 mirror pairs of $Al_{0.9}Ga_{0.1}As$/GaAs and a Bragg wavelength of $\lambda_B = 1060$ nm. Since we are targeting a top-emitting structure it is important that the DBR reflectance is larger than the top HCG reflectance. The reflectivity at λ_B of the DBR is estimated to be 0.9997 and that of the HCG 0.9988, computed by the transfer matrix method and rigorously coupled wave analysis, respectively. These values are based on an estimated loss of 5/cm [15]. The active region consists of $In_{0.3}Ga_{0.7}As$ multiple quantum wells (QWs) placed at the antinode of the electric field intensity at λ_B. The three $In_{0.3}Ga_{0.7}As$ QWs are highly strained and in order to achieve strain compensation $GaAs_{0.8}P_{0.2}$ is used as barrier layers. Current confinement is achieved through oxidizing a 55-nm-thick $Al_{0.98}Ga_{0.02}As$ layer placed at a intensity node. Through 2-D finite-difference time-domain simulations, we have found that an oxide aperture of 8 μm ensures single-mode operation. Fig. 2 shows a plot of the calculated mode profile of the fundamental mode (in dB) [16]. A moderately p-doped GaAs current spreading layer makes up the anode of the pin-junction diode.

In order to reduce the parasitic reflectance at the high-index contrast semiconductor to air interface we employ an Al_2O_3 antireflective coating (ARC) made of oxidized $Al_{0.98}Ga_{0.02}As$ since this allows growth of the device in a single epitaxial step [17]. The nominal refractive index and thickness of the ARC is 1.6 and 171 nm, respectively (a 6.7% thickness reduction during oxidation is accounted for in the epitaxial growth [18]). The final air-gap height of 560 nm is defined by an $In_{0.5}Al_{0.5}P$ sacrificial layer which is removed during processing. The top layer of n-doped GaAs is structured into a HCG mirror. For the HCG, we have chosen a thickness of 280 nm, a period of 460 nm, and a duty cycle of 0.72. A SEM image of the fabricated VCSEL is shown in Fig. 3(a) while a close-up on the MEMS and HCG structure is seen in Fig. 3(b). Further details on the design and processing are found in [19] and [20].

III. Results and Discussion

The VCSELs have been tested in terms of their light–current–voltage characteristics and single-mode property. During device processing, the Bragg wavelength was measured to be $\lambda_B = 1065 \pm 5$ nm and the photoluminescence peak $\lambda_{PL} = 1052 \pm 8$ nm averaged across a 10×10 mm die. Fig. 4 shows a plot of the *I–V* and current-power relation for a HCG VCSEL. The power was measured using a large-area silicon photodiode (Thorlabs FDS1010), as estimated using data for the wavelength-dependent responsivity. The threshold current is around 1 mA and the maximum output power at room-temperature (20 °C) is 0.9 mW. Thermal roll-over is seen to occur at 10 mA and the VCSEL continues to lase up to 60 °C.

Fig. 5 shows a plot of the optical spectrum measured by coupling part of the emission into a Corning SMF-28e fiber connected to an optical spectrum analyzer. The output spectrum shows that the VCSELs are single-mode with a peak emission at 1070 nm. This makes the wavelength detuning between the lasing mode and peak gain/reflectivity around 20 nm. The HCG mirror provide an additional method of higher order mode suppression since its size is comparable to the oxide aperture, hence high-order transverse modes will experience a larger optical loss [17].

The output spectrum was also measured for increasing tuning voltages applied to the MEMS contact; in these measurements, the n-doped MEMS contact was biased at positive polarity with respect to the laser anode. The optical spectrum for increasing MEMS tuning voltage is seen in Fig. 6 with the intensity on the left axis. The 3 dB tuning range is seen to be 10 nm, while the full tuning range is larger than 16 nm. The tuning voltage

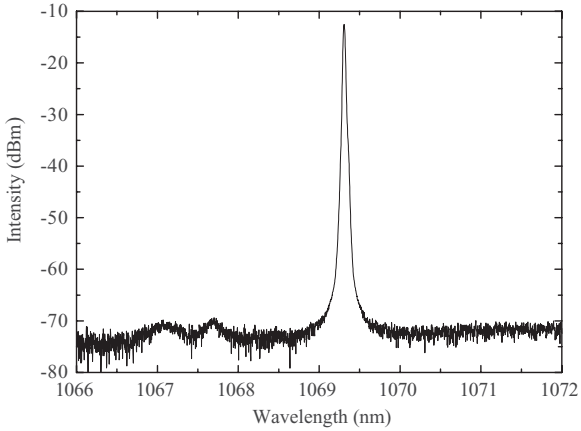

Fig. 5. Optical spectrum at a laser current of 5 mA and no voltage applied to the MEMS contact.

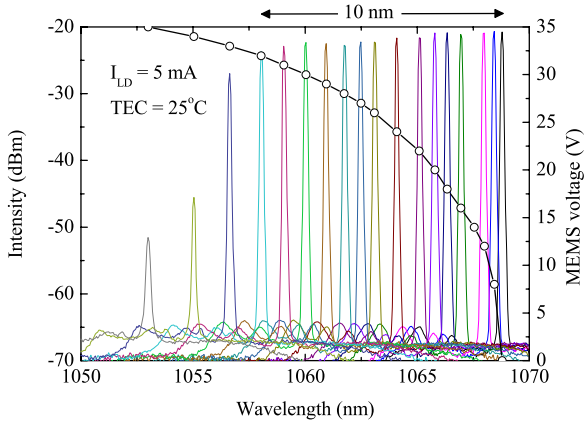

Fig. 6. Optical intensity (left axis) versus wavelength at various MEMS tuning voltages (right axis) using 5 mA laser current. The spectra are taken at 19 discrete tuning voltages from 0 to 35 V. The ○ symbols show the tuning voltage intensity peak wavelength pairs.

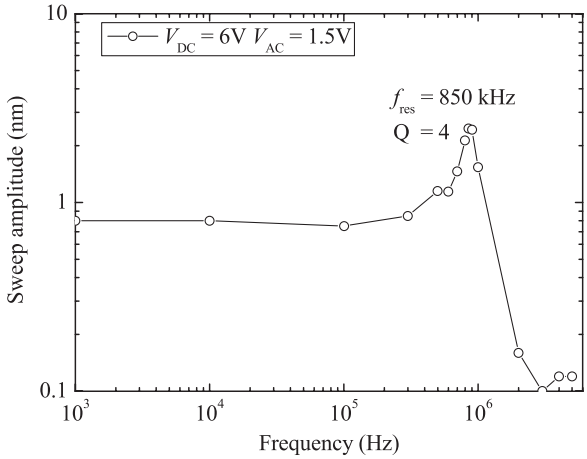

Fig. 7. Wavelength sweep amplitude versus excitation frequency.

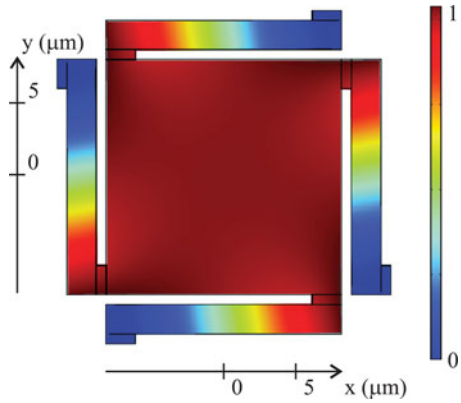

Fig. 8. Fundamental mechanical resonance mode (displacement in arbitrary units). The mirror sidelength is 12 μm, the beam width 1.5 μm, the hinge width 1.5 μm and the thickness 0.28 μm. The fundamental resonance frequency is 841.5 kHz.

is shown on the right axis and the tuning range is found to be limited by pull-in around 35 V. Static pull-in occurs at a displacement, that is, 1/3 of the equilibrium effective MEMS actuator gap $g_0 = g_a + h_r/\epsilon_r$, where g_a is the air gap, h_r and ϵ_r are the thickness and relative permittivity of the ARC layer, respectively.

From measurements on another VCSEL with 18 nm tuning range limited by pull-in at 29 V, we can extract the maximum tuning efficiency to be $\Delta\lambda/\Delta g = 0.08$ nm/nm. Compared to the tuning efficiency of 0.01 nm/nm in [13] a significant increase is achieved by the extended cavity design. A similar increase in the tuning efficiency to 0.14 nm/nm has been reported using a SiON ARC [10].

A continuously swept light source is interesting for OCT and hence both small- and large-signal modulations were investigated. As evident from Fig. 6, even at relatively large tuning voltages the mechanical deflection is small (the mechanical deflection is directly proportional to the wavelength change). The small-signal modulation response of the VCSEL was measured by applying the voltage waveform

$$V(t) = V_{\rm dc} + V_{\rm ac}\cos(\omega t) \quad (1)$$

with $V_{\rm dc} = 6$ V and $V_{\rm ac} = 1.5$ V. The resulting sweep amplitude extracted from the optical spectrum is shown versus the excitation frequency $f = \omega/(2\pi)$ in Fig. 7. The frequency response follows the transfer function of a damped harmonic oscillator with a flat response at low frequencies, a response peak near the mechanical resonance frequency of $f_0 = 850$ kHz, and a steep decline of the response at higher frequencies.

The experimental resonance frequency is in good agreement with the mechanical resonance frequency of 841.5 kHz found from a finite element eigenfrequency analysis using COMSOL Multiphysics. Fig. 8 shows the fundamental mechanical resonance mode of the micromirror. Due to the electrostatic spring softening the resonance frequency will be overestimated in the mechanical model, while leaving out the grating underestimates the resonance frequency. From Fig. 7 the quality factor, $Q = \omega_0/\Delta\omega$, of 4 is extracted. The low quality factor was expected, since the measurements were performed in air at atmospheric pressure where squeeze film damping in the narrow air gap is the dominant loss mechanism contributing to the low quality factor of the MEMS oscillator. Measurements of the thermal vibration spectrum of a micromirror of similar size using a Doppler vibrometry confirmed this expectation, since a

quality factor of 2490 was extracted from the spectrum at reduced pressure using a Lorentzian fit.

In static operation of a MEMS VCSEL, only blue shift (moving toward shorter wavelengths) of the emission wavelength is applicable. Here we show how red shift (moving toward longer wavelengths) as well can be exploited in dynamic operation to increase the tuning range. The use of resonant excitation of the MEMS has been demonstrated by Vail *et al.* for continuously sweeping the wavelength 12 nm for a 980 nm VCSEL [21], [22]. In the following, the theory of the resonant MEMS VCSEL is described. In the MEMS VCSEL, the mirror-spring system is really a mechanical harmonic oscillator with a nonlinear actuation force. The equation of motion for the MEMS [23] may, in dimensionless form, be expressed as

$$\frac{\ddot{u}}{\omega_0^2} + \frac{1}{\omega_0 Q}\dot{u} + u = \frac{4}{27}\left(\frac{V(t)}{V_{\rm PI}}\right)^2 \frac{1}{(1-u)^2} \tag{2}$$

where $u = z/g_0$ is the normalized mirror deflection, Q is the quality factor, $\omega_0 = (K/M)^{1/2}$ is the angular resonance frequency, $V(t)$ the applied actuation voltage, and $V_{\rm PI} = (8g_0^2 K/(27C_0))^{1/2}$ the pull-in voltage; here K is the effective spring constant of the beams supporting the mirror, M is the mass of the mirror, and C_0 is the equilibrium actuator capacitance.

Obviously, eq. (2) is a nonlinear differential equation; the left-hand side is the equation of motion for a linear harmonic oscillator while the right-hand side is a dimensionless nonlinear electrostatic driving force term $F_{\rm el}(u,t)$. The static deflection curve at constant actuation voltage $V(t) = V_{\rm dc}$ is however easily obtained from

$$u(1-u)^2 = \frac{4}{27}\left(\frac{V_{\rm dc}}{V_{\rm PI}}\right)^2 \tag{3}$$

for $u \le 1/3$ and $V_{\rm dc} \le V_{\rm PI}$; at larger deflections and voltages the system becomes unstable and pull-in occurs. The laser wavelength shift as a function of the static actuation voltage observed in Fig. 6 is in perfect agreement with eq. (3).

Inserting eq. (1) into (2) and doing a Taylor expansion of the right-hand side in terms of the normalized deflection u the electrostatic driving force, $F_{\rm el}$ is written as

$$F_{\rm el}(u,t) = \frac{4\omega_0^2}{27V_{\rm PI}}\left(1 + 2u + 3u^2 + 4u^3 + \mathcal{O}(u^4)\right) \times \left(V_{\rm dc}^2 + \frac{V_{\rm ac}^2}{2} + 2V_{\rm ac}V_{\rm dc}\cos(\omega t) + \frac{V_{\rm ac}^2}{2}\cos(2\omega t)\right). \tag{4}$$

Since $|u| < 1$ the higher order terms can be ignored for sufficiently small deflections, and then to first order the MEMS will behave as a linear forced oscillator. The first higher order term $(2u)$ results in the reduction of the effective spring constant, an effect commonly referred to as electrostatic spring softening. The main effect of the spring softening term is a reduction of the resonance frequency with increasing dc actuation voltage.

From (4), it is further seen that due to the quadratic dependence of the force on the voltage a sinusoidal drive waveform will always cause a dc offset force, and a corresponding dc offset deflection. Furthermore, there is a force component at the drive frequency ω and a second harmonic component at 2ω. If the structure allows bipolar modulation voltages, a sinusoidal drive voltage at half the resonance frequency $\omega = \omega_0/2$ without an applied dc voltage, will cause the second harmonic term to be dominant and modulation at ω missing.

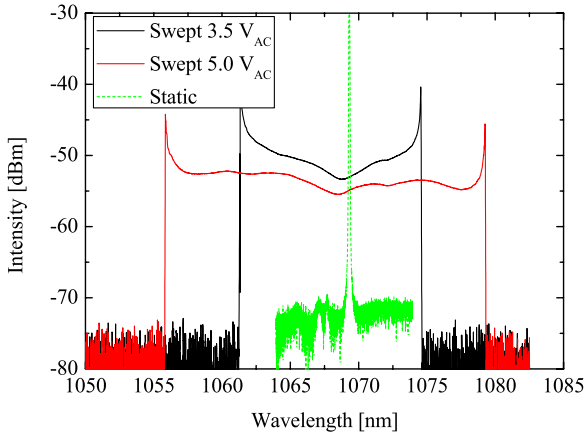

Fig. 9. Optical spectrum at a laser current of 7 mA in static operation at $V_{\rm dc} = 10$ V (dashed line), and swept at 850 kHz at $V_{\rm dc} = 10$ V and $V_{\rm ac} = 3.5$ and 5 V (solid lines).

On the other hand, by choosing $V_{\rm ac} \ll V_{\rm dc}$ the excitation of the second harmonic term can be suppressed and the ac force will be dominated by the term at the excitation frequency. For the linear harmonic oscillator, a forced oscillation will result in the steady-state time-dependent deflection [23]

$$u(t) = \frac{4}{27}\frac{2V_{\rm ac}V_{\rm dc}}{V_{\rm PI}^2}\frac{\omega_0^2\cos(\omega t - \phi)}{\sqrt{\left(\omega_0^2 - \omega^2\right)^2 + (\omega_0\omega/Q)^2}} + u_0 \tag{5}$$

which has a peak near $\omega = \omega_0$ and with a frequency dependent phaselag of ϕ between forcing and oscillation. Equation (5) describes the frequency dependence of the sweep amplitude seen in Fig. 7. The relative deflection u will be both positive and negative and the amplitude depends on the product of the ac modulation voltage and the dc offset voltage as well as on the frequency.

Fig. 9 shows the optical spectra of the VCSEL in static and dynamic operations with $V_{\rm dc} = 10$ V and $V_{\rm ac} = 0$, 3.5, and 5 V. The initial wavelength is 1069 nm and from Fig. 6 it is seen that changing $V_{\rm dc}$ from 10 to 13.5 V changes the static wavelength from 1069 to 1068 nm. When the VCSEL mirror is driven at the mechanical resonance frequency the wavelength is seen to both blue- and red-shift as evident in Fig. 9, where the total wavelength sweep amplitude is 14 nm at $V_{\rm ac} = 3.5$ V. Increasing the ac voltage to 5 V increases the wavelength sweep amplitude to 24 nm, which is more than the 3 dB tuning range in static operation. In Fig. 9, the center wavelength in dynamic operation (at highest speed and thus lowest integrated intensity) blue-shift for increasing sweep ac voltage as expected from (4) and (5). The constant electrostatic force term in (4) causes a constant off-set u_0 from the resting position; the off-set depends on both the dc and the ac voltages. Hence, in order to achieve the maximum tuning range it is advantageous to use a small ac voltage and very low dc voltage to minimize the offset.

IV. Conclusion

The static and dynamic performances of a tunable 1060 nm VCSEL with extended cavity has been presented. The top DBR mirror of the VCSEL was substituted with a HCG mirror to make the VCSEL polarization stable. The VCSEL shows 0.9 mW peak output power at room-temperature operation with high side-mode suppression. The static 3 dB tuning range is 10 nm and the dynamic 3 dB tuning range 24 nm. The increased dynamic tuning range is achieved by driving the MEMS at resonance, which makes the wavelength both blue- and red-shift. As shown, the bipolar deflection of the mirror can be used to double the tuning range of swept source lasers.

Acknowledgment

The authors would like to thank Silvan Schmidt, DTU Nanotech, for help with the Laser Doppler Vibrometry measurements. Center for Individual Nanoparticle Functionality (CINF) is sponsored by The Danish National Research Foundation (DNRF54).

References

[1] H. Nasu, "Short-reach optical interconnects employing high-density parallel-optical modules," *IEEE J. Sel. Topics Quantum Electron.*, vol. 16, no. 5, pp. 1337–1346, Sep. 2010.

[2] B. Potsaid, V. Jayaraman, J. G. Fujimoto, J. Jiang, P. J. S. Heim, and A. E. Cable, "MEMS tunable VCSEL light source for ultrahigh speed 60 kHz-1MHz axial scan rate and long range centimeter class OCT imaging," in *Proc. SPIE*, vol. 8213, San Francisco, CA, USA, 2012, pp. 1–8.

[3] H. P. Zappe, M. Hess, M. Moser, R. Hövel, K. Gulden, H.-P. Gauggel, and F. Monti di Sopra, "Narrow-linewidth vertical-cavity surface-emitting lasers for oxygen detection," *Appl. Opt.*, vol. 39, no. 15, pp. 2475–2479, May 2000.

[4] B. Kögel, H. Halbritter, S. Jatta, M. Maute, G. Böhm, M.-C. Amann, M. Lackner, M. Schwarzott, F. Winter, and P. Meissner, "Simultaneous spectroscopy of NH3 and CO using a $>$ 50 nm continuously tunable MEMS-VCSEL," *IEEE Sensors J.*, vol. 7, no. 11, pp. 1483–1489, Nov. 2007.

[5] B. Považay, B. Hermann, V. Kajić, B. Hofer, and W. Drexler, "High speed, spectrometer based optical coherence tomography at 1050 nm for isotropic 3-d OCT imaging and visualization of retinal and choroidal vasculature," in *Proc. Biomed. Opt. OCT Opthalmic Appl.*, St. Petersburg, FL, USA, 2008, pp. 041211-1–041211-7.

[6] I. Grulkowski, J. J. Liu, B. Potsaid, V. Jayaraman, C. D. Lu, J. Jiang, A. E. Cable, J. S. Duker, and J. G. Fujimoto, "Retinal, anterior segment and full eye imaging using ultrahigh speed swept source OCT with vertical-cavity surface emitting lasers," *Bio. Opt. Exp.*, vol. 3, no. 11, pp. 2733–2751, Oct. 2012.

[7] M. S. Wu, E. C. Vail, G. S. Li, W. Yuen, and C. J. Chang-Hasnain, "Tunable micromachined vertical cavity surface emitting laser," *Electron. Lett.*, vol. 31, no. 19, pp. 1671–1672, Sep. 1995.

[8] F. Sugihwo, M. C. Larson, and J. S. Harris Jr., "Micromachined widely tunable vertical cavity laser diodes," *J. Microelectromech. Syst.*, vol. 7, no. 1, pp. 48–55, Mar. 1998.

[9] L. Fan, M. C. Wu, H. C. Lee, and P. Grodzinski, "10.1 nm range continuous wavelength-tunable vertical-cavity surface-emitting lasers," *Electron. Lett.*, vol. 30, no. 17, pp. 1409–1410, Aug. 1994.

[10] C. Gierl, T. Gruendl, P. Debernardi, K. Zogal, C. Grasse, H. A. Davani, G. Böhm, S. Jatta, F. Küppers, P. Meißner, and M.-C. Amann, "Surface micromachined tunable 1.55 μm-VCSEL with 102 nm continuous single-mode tuning," *Opt. Exp.*, vol. 19, no. 18, pp. 17336–17343, Aug. 2011.

[11] V. Jayaraman, G. D. Cole, M. Robertson, A. Uddin, and A. Cable, "High-sweep-rate 1310 nm MEMS-VCSEL with 150 nm continuous tuning range," *Electron. Lett.*, vol. 48, no. 14, pp. 867–869, Jul. 2012.

[12] V. Jayaraman, G. D. Cole, M. Robertson, C. Burgner, D. John, A. Uddin, and A. Cable, "Rapidly swept, ultra-widely-tunable 1060 nm MEMS-VCSELs," *Electron. Lett.*, vol. 48, no. 21, pp. 1331–1333, Oct. 2012.

[13] M. C. Y. Huang, Y. Zhou, and C. J. Chang-Hasnain, "Nano electromechanical optoelectronic tunable VCSEL," *Opt. Exp.*, vol. 15, no. 3, pp. 1222–1227, Feb. 2007.

[14] I.-S. Chung, V. Iakovlev, A. Sirbu, A. Mereuta, A. Caliman, E. Kapon, and J. Mørk, "Broadband MEMS-tunable high-index-contrast subwavelength grating long-wavelength VCSEL," *IEEE J. Quantum Electron.*, vol. 46, no. 9, pp. 1245–1253, Sep. 2010.

[15] W. G. Spitzer and J. M. Whelan, "Infrared absorption and electron effective mass in n-type gallium arsenide," *Phys. Rev.*, vol. 114, no. 1, pp. 59–63, Apr. 1959.

[16] I.-S. Chung, J. Mørk, P. Gilet, and A. Chelnokov, "Subwavelength grating-mirror VCSEL with a thin oxide gap," *IEEE Photon. Technol. Lett.*, vol. 20, no. 2, pp. 105–107, Jan. 2008.

[17] H. Sano, A. Matsutani, and F. Koyama, "Athermal and tunable operations of 850 nm VCSEL with thermally actuated cantilever structure," in *Proc. 35th Eur. Conf. Opt. Commun.*, Vienna, Austria, 2009, P2.26, pp. 1–2.

[18] K. D. Choquette, K. M. Geib, C. I. H. Ashby, R. D. Twesten, O. Blum, H. Q. Hou, D. M. Follstaedt, B. E. Hammons, D. Mathes, and R. Hull, "Advances in selective wet oxidation of AlGaAs alloys," *IEEE J. Sel. Topics Quantum Electron.*, vol. 3, no. 3, pp. 916–926, Jun. 1997.

[19] T. Ansbæk, I.-S. Chung, E. S. Semenova, and K. Yvind, "1060 nm tunable monolithic high index contrast subwavelength grating VCSEL," *Photon. Technol. Lett.*, vol. 25, no. 4–4, pp. 365–367, Feb. 2013.

[20] T. Ansbæk, E. S. Semenova, K. Yvind, and O. Hansen, "Crystallographic dependence of the lateral undercut wet etch rate of $Al_{0.5}In_{0.5}P$ in diluted HCl for III-V sacrificial release," *J. Vac. Sci. Technol. B.*, vol. 31, no. 1, pp. 011209-1–011209-4, Jan. 2013.

[21] E. C. Vail, G. S. Li, W. Yuen, and C. J. Chang-Hasnain, "Novel self-chirped VCSEL with a micromechanical resonator," in *Proc. 15th Int. Semicond. Laser Conf.*, Haifa, Israel, Oct. 1996, pp. 181–182.

[22] E. C. Vail, G. S. Li, W. Yuen, and C. J. Chang-Hasnain, "High performance and novel effects of micromechanical tunable vertical-cavity lasers," *IEEE J. Sel. Topics Quantum Electron.*, vol. 3, no. 2, pp. 691–697, Apr. 1997.

[23] S. D. Senturia, *Microsystem Design*. Boston, MA, USA: Kluwer, 2001.

Thor Ansbæk was born in Copenhagen, Denmark, in 1984. He received the M.Sc. Eng. degree in 2008 and the Ph.D. degree in 2012 both at The Technical University of Denmark, Kongens Lyngby, Denmark.

His research interests include semiconductor fabrication, microelectromechanical systems, and vertical-cavity surface-emitting lasers for medical diagnosis.

Il-Sug Chung received the B.Sc. and M.Sc. degrees in physics from the Korea Advanced Institute of Science and Technology, Daejeon, Korea, and the Ph.D. degree in optoelectronics from the Gwangju Institute of Science and Technology, Gwangju, Korea, in 1997, 2000, and 2006, respectively.

Since 2006, he has been with the Department of Photonics Engineering, Technical University of Denmark, Kongens Lyngby, Denmark, and is currently an Associate Professor. His research interests include modeling, fabrication, and characterization of hybrid III-V-on-Si lasers and detectors, novel VCSELs, subwavelength gratings, and photonic crystal lasers for silicon photonics, sensing, high-speed optical communications including space-division and mode-division multiplexing.

Elizaveta S. Semenova received the M.Sc. degree from St.-Petersburg State Technical University, Russia, in 2001, and the Ph.D. degree in semiconductors physics from the Laboratory of Physics of Semiconductor Heterostructures, Ioffe Physico-Technical Institute, Russia, in 2005.

She is an Assistant Professor at DTU Fotonik, the Technical University of Denmark, Kongens Lyngby, Denmark. Her research interests include mainly design and fabrication epitaxial heterostructures for optoelectronic applications, in particular edge-emitting and surface emitting (VCSELs) lasers (for 980–1550 nm wavelength region), microcavities, single photon emitters and photonic crystals; and microelectronic applications such as high electron mobility transistors.

Ole Hansen received the M.Sc. degree in microtechnology from Technical University of Denmark, Kongens Lyngby, Denmark, in 1977.

Since then, he has worked with micro- and nanotechnology and applications of the technology within electronics, metrology, sensing, catalysis, and energy harvesting. He is a Professor at DTU Nanotech, the Technical University of Denmark, where he is the Head of the Silicon Microtechnology Group, with activities within lithography-based micro- and nanotechnology. His current research interests include photo-catalysis and tools for characterizing catalytic processes. Since 2005, he has been part of the Danish National Research Foundation Center CINF, Center for Individual Nanoparticle Functionality.

Kresten Yvind received the M.Sc.E. and Ph.D. degrees in 1999 and 2003 from the Research Center for Communication, Optics and Materials (COM), Technical University of Denmark, Kongens Lyngby, Denmark.

He is currently an Associate Professor and the Group Leader for Nanophotonic Devices at DTU Fotonik, Kongens Lyngby. His working areas cover a broad range of topics from design, cleanroom fabrication, and testing of optical devices in InP, GaAs, and silicon.